Research article

Tuo Qu, Fang Liu*, Yuechai Lin, Kaiyu Cui, Xue Feng, Wei Zhang and Yidong Huang*

Cherenkov radiation generated in hexagonal boron nitride using extremely low-energy electrons

https://doi.org/10.1515/nanoph-2020-0090
Received February 6, 2020; accepted April 13, 2020

Abstract: Cherenkov radiation (CR) is the electromagnetic shockwaves generated by the uniform motion of charged particles at a velocity exceeding the phase velocity of light in a given medium. In the Reststrahlen bands of hexagonal boron nitride (hBN), hyperbolic phonon polaritons (HPPs) are generated owing to the coupling between mid-infrared electromagnetic waves and strong anisotropic lattice vibrations. This study theoretically and numerically investigates the generation of volume CR based on HPPs in hBN with super-large wavevectors. Results reveal that CR can be generated using free electrons with an extremely low kinetic energy of 1 eV—two orders of magnitude lower than that reported in extant studies. The findings of this investigation provide new insights into significantly reducing the electron energy required for CR generation and potentially open new research avenues in the fields of CR and HPP.

Keywords: Cherenkov radiation; hexagonal boron nitride (hBN); hyperbolic materials; phonon polaritons.

***Corresponding authors: Fang Liu and Yidong Huang**, Department of Electronic Engineering, Tsinghua University, Beijing, 100084, PR China; Beijing National Research Center for Information Science and Technology, Tsinghua University, Beijing, 100084, PR China; Beijing Academy of Quantum Information Science, Beijing, 100193, PR China, E-mail: liu_fang@tsinghua.edu.cn (F. Liu); yidonghuang@tsinghua.edu.cn (Y. Huang)
Tuo Qu, Yuechai Lin, Kaiyu Cui, Xue Feng and Wei Zhang: Department of Electronic Engineering, Tsinghua University, Beijing, 100084, PR China; Beijing National Research Center for Information Science and Technology, Tsinghua University, Beijing, 100084, PR China; and Beijing Academy of Quantum Information Science, Beijing, 100193, PR China. https://orcid.org/0000-0002-5196-7196 (T. Qu)

1 Introduction

Cherenkov radiation (CR) refers to the electromagnetic shockwaves generated by charged particles moving with a uniform velocity exceeding the phase velocity of light in a given medium [1, 2]. In 1958, for the discovery and explanation of CR, Pavel A. Cherenkov, Il´ja M. Frank, and Igor Y. Tamm were jointly awarded the Nobel Prize in physics [3–5]. CR has since been employed in several applications, including particle detection [6], free-electron lasers [7], medical imaging [8], and phototherapy [9].

Recently, many interesting phenomena of CR have been reported by utilizing free electrons to interact with various nanostructures and nanomaterials, such as plasmonic structures [10, 11], two dimensional materials [12–15], and metamaterials [16, 17]. Among these works, CR generation using low-energy electrons, which makes the on-chip integrated free-electron emitters available for generation of CR with high efficiency, has received increased research attention in recent years [16, 18–22]. Abajo theoretically studied the excitation of propagating and localized plasmons of graphene with electron energy as low as 100 eV [19]. Our group experimentally demonstrated CR generation by electrons with energies in the range of 0.25–1.4 keV, which utilized the hyperbolic plasmonic modes in multilayered structures [16]. Smith–Purcell radiation (SPR), which is essentially a kind of CR [23], can also be excited by low-energy electrons. For examples, Massuda et al. demonstrated experimentally the 1.5–6 keV excited SPR [21], and Roques–Carmes et al. accomplished SPR generation using CMOS-compatible, all-silicon gratings with electron energies in the range of 2–20 keV [22].

For hyperbolic metamaterials (HMMs), the electromagnetic wave with infinitely large wavevectors could be supported [24]. Thus, no matter how small the velocity v_0 (energy E) of free electrons is, the evanescent waves surrounding free electrons with wavevector $k_e = 2\pi \cdot f / v_0$ (f is the frequency of evanescent waves and v_0 is the velocity of free electrons) [18] could be coupled into HMMs and CR

could be generated [16, 25]. However, in practice, the plasmonic metal/dielectric multilayered structure could not be considered as perfect HMM with infinitely large wavevectors if its unit size does not satisfy the subwavelength condition [24]. In other words, the minimum unit size determines the largest wavevector of electromagnetic waves propagating in the multilayered structure [24], as well as the lowest electron velocity (energy) for generating CR in the multilayered structure [16]. The lower the electron energy is, the thinner layer is demanded for CR generation. For example, utilizing free electrons with energy E = 10 eV to generate CR, each layer in Au/SiO_2 multilayers must merely be several angstrom-meters thick to satisfy the subwavelength condition, since the CR wavelength (λ_{CR}) is estimated to be only ~3 nm at frequency f = 600 THz (corresponding to vacuum wavelength λ_0 = 500 nm). Such Au/SiO_2 multilayer structure could hardly be realized in reality. In addition, the high metal loss caused by strong mode confinement of short λ_{CR} in multilayered HMMs [24, 26, 27] is another practical obstacle. Namely, there is a bottleneck hindering generation of CR in common HMMs with lower electron velocities (energies).

The above-mentioned challenges can be overcome by replacing the plasmonic modes in multilayer structures with hyperbolic phonon polaritons (HPPs) in hexagonal boron nitride (hBN). Phonon polaritons, which represent coupling modes between electromagnetic waves and lattice vibrations in polar dielectrics, were first proposed and investigated by K. Huang in 1951 [28, 29]. HPPs within the Reststrahlen band of hBN were first investigated by Dai et al. in 2014 [30], post which they have attracted increased research interest owing to their extraordinary properties—low damping [31], strong mode confinement [32], and easy hybridization with graphene plasmons [33, 34]. These properties have facilitated the realization of deep subdiffraction waveguides [35], nano-imaging [36], hyperbolic metasurfaces [37, 38], and heat transfer enhancement [39]. The bottleneck of reduction of electron velocity (energy) for CR generation in common HMMs can be overcome in hBN, because hBN is a natural hyperbolic material with atomic-layer thickness—a size that HMMs can hardly achieve. For this reason, HPPs in hBN can support much larger wavevectors, and the electron energy required for CR generation can be significantly reduced.

This paper theoretically and numerically investigates the generation of volume CR based on HPPs inside hBN using free electrons of extremely low energies. The results reveal that the free-electron energy can be greatly reduced to 1 eV. Compared with the lowest electron energy (100 eV) for generation of volume CR inside plasmonic multilayer structure [16] and surface CR at vacuum–hBN interface [40], the value in this paper is about two orders of magnitude lower. It is also found that the CR power produced by electrons with 1-eV energy exceeds that generated by electrons with 100-eV energy. The authors believe that the findings of this study offer a viable method for significant reduction of the electron energy required for CR generation.

2 Results

Figure 1A illustrates the schematic of volume CR generation when an electron bunch passes over the hBN thin film. Since hBN is a naturally occurring hyperbolic material that supports HPPs [30], CR could be excited by free electrons with extremely low energy due to the coupling from evanescent waves surrounding the electron bunch to the propagating HPP waves in hBN.

For simulation of the generation of CR within hBN, the permittivity of hBN can be obtained according to [41]

$$\varepsilon_m = \varepsilon_{\infty,m}\left(1 + \frac{\omega_{LO,m}^2 - \omega_{TO,m}^2}{-\omega^2 + \omega_{TO,m}^2 - i\omega\gamma_m}\right), \tag{1}$$

where m denotes the out-of-plane direction x or in-plane direction y/z of hBN films. Values of parameters used in Equation (1) are obtained from extant studies [30, 42, 43]. In particular, values of certain parameters depend on the phonon modes—A_{2u} and E_{1u} [44]. In the out-of-plane A_{2u} phonon mode, the frequency of the transverse optical (TO) phonon is $\omega_{TO,x}$ = 783 cm^{-1}, whereas that of the longitudinal optical (LO) phonon is $\omega_{LO,x}$ = 828 cm^{-1} [42]. Likewise, in the in-plane E_{1u} phonon mode, corresponding values of TO and LO frequencies are given by $\omega_{TO,y/z}$ = 1367 cm^{-1} and $\omega_{LO,y/z}$ = 1610 cm^{-1}, respectively [42]. Additionally, values of the high-frequency permittivity are given by $\varepsilon_{\infty,x}$ = 2.95 and $\varepsilon_{\infty,y/z}$ = 4.87 [43], and damping constants are set as γ_x = 4 cm^{-1} and $\gamma_{y/z}$ = 5 cm^{-1} [30].

Figure 1B plots the real part of the permittivity of hBN against frequency values in the range of 500–2000 cm^{-1}. In the given frequency range, there exist two Reststrahlen bands derived from the two phonon modes A_{2u} and E_{1u}, respectively. The lower- and higher-frequency Reststrahlen bands correspond to type-I ($\varepsilon_x < 0$ and $\varepsilon_{y/z} > 0$) and type-II ($\varepsilon_x > 0$ and $\varepsilon_{y/z} < 0$) hyperbolic regions shaded in red and blue, respectively. In both regions, the iso-frequency surface in wavevector space corresponds to a hyperboloid, which can be expressed as

$$\frac{k_x^2}{\varepsilon_{y/z}} + \frac{k_y^2 + k_z^2}{\varepsilon_x} = k_0^2, \tag{2}$$

where k_x and $k_{y/z}$ denote the wavevectors in the out-of-plane direction x and in-plane direction y/z, respectively,

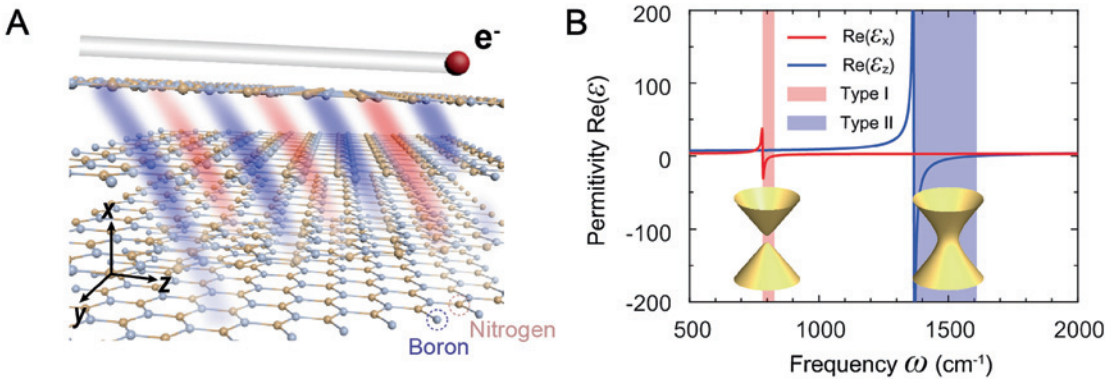

Figure 1: (A) Schematic of volume Cherenkov radiation (CR) generation in hBN using an electron bunch; (B) Real part of hBN permittivity within frequency range $\omega = 500–2000\ \text{cm}^{-1}$. Shaded areas refer to type-I and type-II hyperbolic regions. Insets demonstrate iso-frequency surfaces at $\omega = 800\ \text{cm}^{-1}$ and $\omega = 1500\ \text{cm}^{-1}$.

and k_0 denotes the wavevector in vacuum. As observed, the iso-frequency surface is a double-sheeted hyperboloid at $\omega = 800\ \text{cm}^{-1}$ and single-sheeted hyperboloid at $\omega = 1500\ \text{cm}^{-1}$, both of which are depicted in the inset of Figure 1B.

When CR is excited by free electrons with energy $E = 1$ eV, we assume that hBN could be treated as a perfect hyperbolic material, namely the subwavelength condition is satisfied. According to $\lambda_{CR} = \lambda_0/\sqrt{\varepsilon_z + (1 - \varepsilon_z/\varepsilon_x)(c/v_0)^2}$ (λ_0 is the wavelength in vacuum and c is the velocity of light in vacuum) [16] and the permittivity in Figure 1B, the wavelength of volume CR generated within hBN is $\lambda_{CR} \approx 8.3$ nm at $\omega = 1500\ \text{cm}^{-1}$. Because the atomic-layer thickness of hBN is only $T_{hBN} = 0.33$ nm [45], which is smaller than $\lambda_{CR}/10$, the above assumption is valid and hBN can be treated as a perfect hyperbolic material for $E = 1$ eV at $\omega = 1500\ \text{cm}^{-1}$. Figure 2 depicts the hyperbolic iso-frequency contours at frequencies $\omega = 800\ \text{cm}^{-1}$ and $\omega = 1500\ \text{cm}^{-1}$, and the wavevector matching between evanescent waves surrounding the low-energy electron bunch and propagating HPP waves in hBN is also indicated. The green arrows (k_e) represent the wavevectors of evanescent waves surrounding free electrons having energy $E = 1$ eV. Based on the wavevector matching depicted in Figure 2, the magnitudes and directions of CR wavevectors (k_{CR}) can be obtained, and the directions of Poynting vectors of CR (S_{CR}) are also labeled.

To verify the above theoretical result, numerical simulations are performed. The simulation adopts the particle-in-cell finite-difference time-domain (PIC-FDTD) method

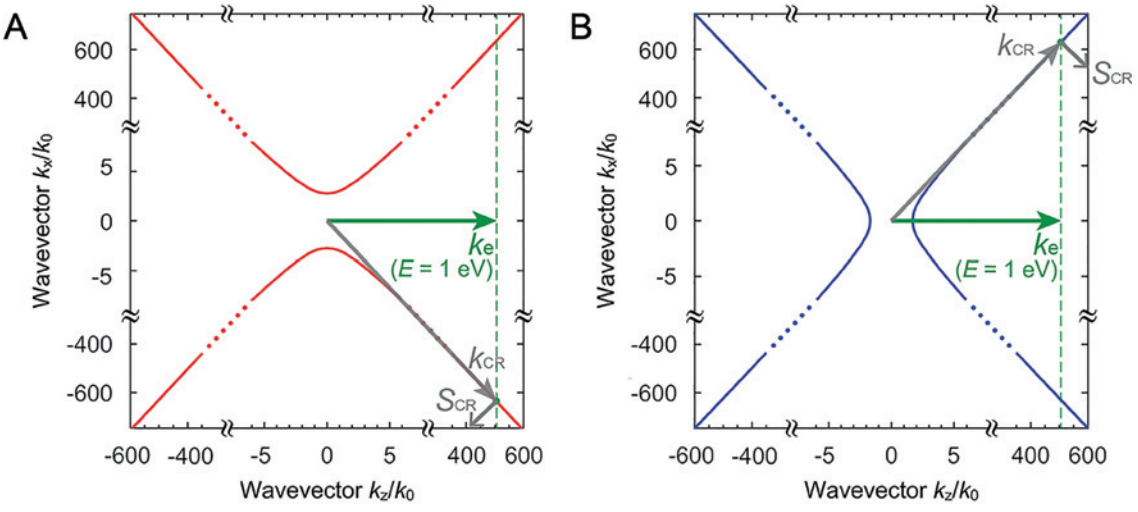

Figure 2: Wavevectors of CR in hBN at frequencies (A) $\omega = 800\ \text{cm}^{-1}$ and (B) $\omega = 1500\ \text{cm}^{-1}$. Red and blue curves are iso-frequency contours for HPP-based CR at the two frequencies, respectively. Green arrows k_e represent wavevectors of evanescent waves surrounding free electrons with energy $E = 1$ eV. Through wavevector matching, wavevectors of CR (k_{CR}) in hBN can be obtained. Directions of Poynting vectors of CR (S_{CR}) are also labeled.

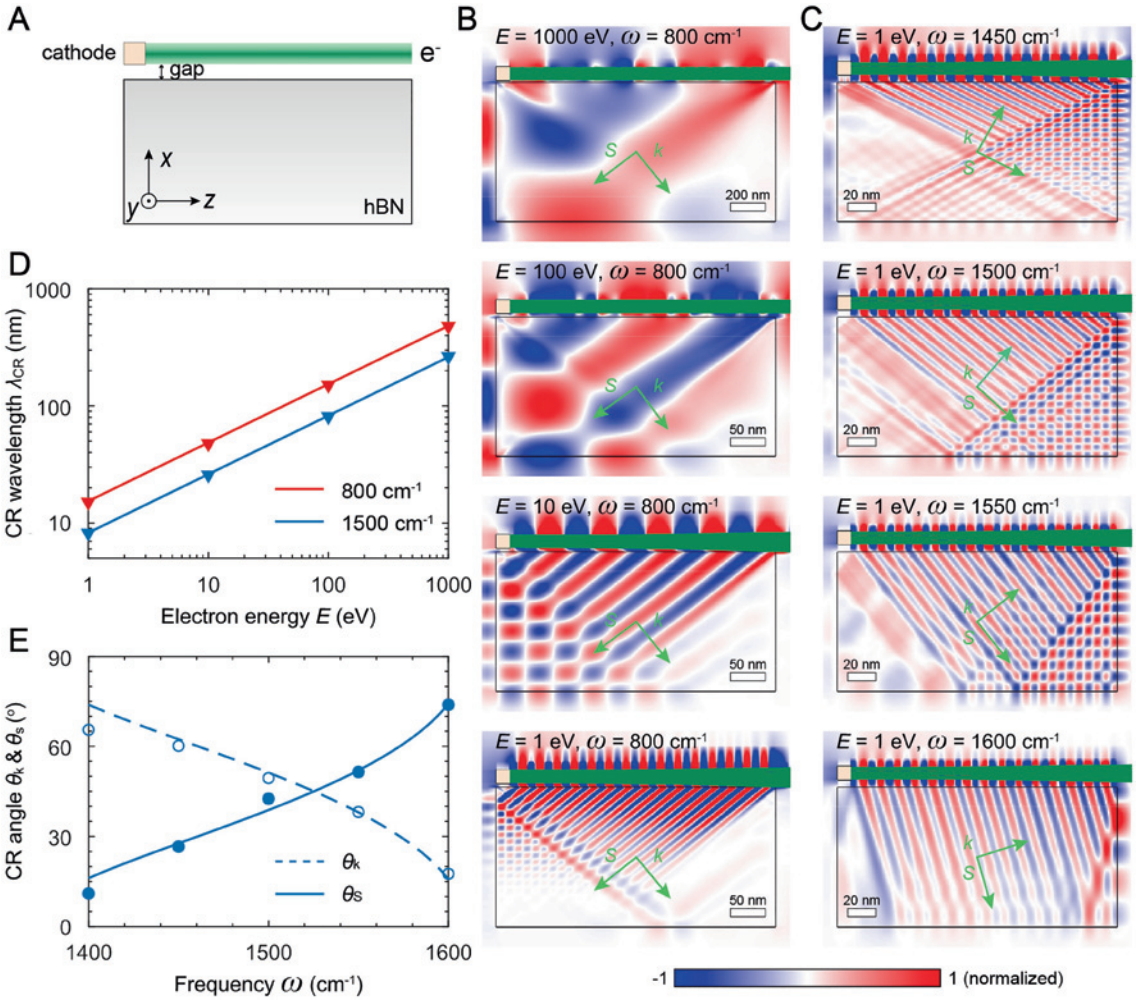

Figure 3: (A) Schematic of simulation model; (B) CR (E_z field component) at frequency $\omega = 800$ cm^{-1} generated using electron energies $E = 1000$, 100, 10, and 1 eV; (C) CR (E_z field component) generated at frequencies $\omega = 1450$, 1500, 1550, and 1600 cm^{-1} with electron energy $E = 1$ eV; (D) Simulated (triangles) and analytical (lines) results of CR wavelengths in hBN with electron energies varying in the range $E = 1$–1000 eV at frequencies $\omega = 800$ cm^{-1} (red) and $\omega = 1500$ cm^{-1} (blue); (E) Simulated (circles) and analytical (lines) results of CR angles in hBN with frequencies of $\omega = 1400$–1600 cm^{-1} when electron energy $E = 1$ eV.

[46], instead of performing dipole array approximations [40]. Thus, the results are more precise and particle dynamics of free electrons could be accounted for. In the simulation, the loss of hBN is considered (see first section of Supplementary Material).

The schematic in Figure 3A depicts the side view (x–z plane) of the three-dimensional simulation model employed in this study. An electron bunch is emitted from the cathode and passes over the hBN film. The charge density of the electron bunch is set to 4×10^{-5} C/m^2 when E equals 1000, 100 and 10 eV, and is reduced to 4×10^{-6} C/m^2 when $E = 1$ eV. Because the evanescent waves surrounding the electron bunch decay rapidly at low electron energies [47], the size of electron–hBN gap is only set to 5 nm. The hBN film along y-axis is considered relatively long. The simulated results of CR are all obtained in the x–z plane cutting through the center of the electron bunch.

Figure 3B,C depict the simulated electric field (E_z) of HPP-based CR in hBN. Amplitudes of E_z are normalized with respect to the maximum values in each case. With the frequency fixed in the type-I hyperbolic region ($\omega = 800$ cm^{-1}), CR can be reliably generated in hBN at electron-energy values of $E = 1000$, 100, 10, and 1 eV. It can be seen that CR could be derived even E is decreased to an extremely low value. When fixing electron energy at $E = 1$ eV, Figure 3C illustrates that CR is generated over the entire type-II hyperbolic region ($\omega = 1450$, 1500, 1550, and 1600 cm^{-1}). Simulation results reveal that CR can be generated in both type-I and type-II regions using electrons with energy values as low as $E = 1$ eV, which is two orders of

magnitude lower compared with that reported in extant literature [16, 40]. The two-dimensional periodic patterns in hBN result from the interference between incident and reflected CR. The green arrows S and k represent the directions of Poynting vectors and wavevectors of the generated CR, respectively.

Moreover, because the PIC-FDTD method can simulate particle dynamics as well [46], Figure 3B,C depict acquired trajectories of electron bunches (marked in green) above the hBN surface. Attention should be paid to the electron bunch expansion, especially at the electron energies $E = 1$ and 10 eV. The said expansion can also be observed in the profile of the evanescent field surrounding the electrons. During the simulation, both the charge density of electron bunch and size of electron–hBN gap are optimized to ensure that the evanescent field of free electrons can be coupled into hBN efficiently and that the expanded electron bunch does not strike the hBN surface.

As discussed in the introduction section, hBN is considered as an ideal hyperbolic material because the subwavelength condition is met for electron energy as low as 1 eV. Moreover, we construct an hBN-equivalent multilayer HMM to study the influence of layer thickness on CR generation and double check whether hBN with atomic-thick layer could support CR excited by 1 eV-electrons or not. Detailed model and calculations support the beginning subwavelength condition (see second section of Supplementary Material). Thus, the nonlocality originated from the structural periodicity [48] can be ignored in our simulation. By the way, the thickness of hBN film T is much larger than the CR wavelength in simulation, so that T is not relevant to the generation of volume CR based on HPP. However, when the thickness T is comparable with the CR wavelength, the eigenmodes of HPP supported by the hBN film should be considered (see third section of Supplementary Material).

Analytical values of CR wavelengths λ_{CR} are calculated using equation $\lambda_{CR} = \lambda_0/\sqrt{\varepsilon_z + (1 - \varepsilon_z/\varepsilon_x)(c/v_0)^2}$ [16], which indicates the distance between two adjacent equiphase surfaces of CR. Different from CR in isotropic media, λ_{CR} inside hBN is related not only to the velocity of electrons but also to both the in-plane and out-of-plane permittivity ε_z and ε_x. Figure 3D depicts the simulated (triangles) and analytical (lines) values of λ_{CR} with the electron energy in the range of $E = 1$–1000 eV, indicating that the simulated results are consistent with their analytical counterparts. More importantly, this verifies that the lower the electron energy is, the shorter the λ_{CR} value could be obtained. Consequently, a super-high integration level of CR devices can be expected.

Figure 3D,E compare the simulated and analytical results of wavelengths and angles of HPP-based CR in hBN to confirm the validity of the simulation results under the condition of extremely low electron energies.

Radiation angles θ_s and θ_k are also key features of CR. θ_s refers to the angle between the direction of electron motion (z-axis) and that of the Poynting vector S_{CR}, whereas θ_k denotes the angle between the direction of electron motion (z-axis) and that of the wavevector k_{CR}. Analytical expressions for θ_s and θ_k are described by [16]

$$\tan(\theta_k) = \sqrt{\varepsilon_z\left[\left(\frac{v_0}{c}\right)^2 - \frac{1}{\varepsilon_x}\right]}, \quad \tan(\theta_s) = \frac{\varepsilon_x}{\varepsilon_z}\tan(\theta_k). \tag{3}$$

As depicted by Equation (3), it is worth noting that the directions of the Poynting vectors S_{CR} and wavevectors k_{CR}

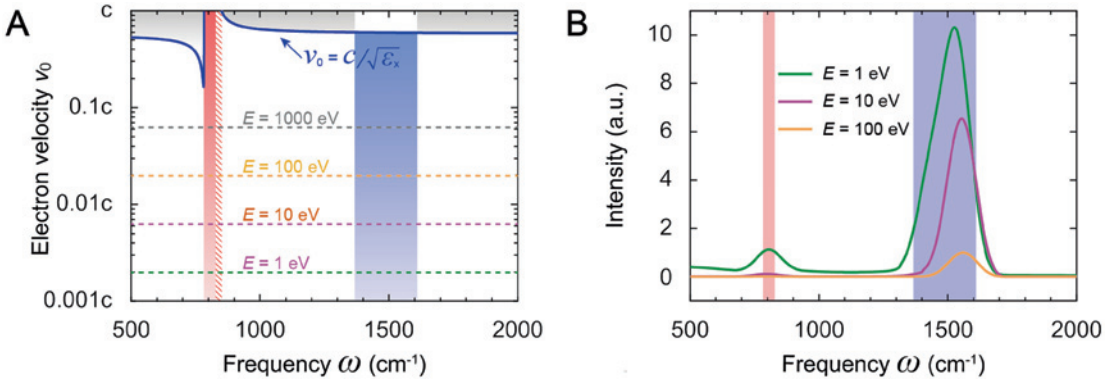

Figure 4: (A) Regions with frequency ω and electron velocity v_0 for CR generation in hBN. CR generation occurs in red- and blue-shaded hyperbolic-dispersion regions with $v_0 < c/\sqrt{\varepsilon_x}$ as well as three gray-shaded elliptical-dispersion regions with $v_0 > c/\sqrt{\varepsilon_x}$. There exists a CR forbidden region (marked with red oblique lines) where no CR can generate; (B) Simulated power spectra of CR generated at $E = 1$, 10, and 100 eV corresponding to the dotted lines in (A).

of the volume CR in hBN are usually not parallel, which are determined by the electron velocity and both the in-plane and out-of-plane permittivity ε_z and ε_x. Figure 3E plots the simulated (circles) and analytical (lines) values of θ_s and θ_k in hBN in the frequency range of ω = 1400–1600 cm^{-1} at fixed electron energy E = 1 eV. The simulated values are in good agreement with their analytical counterparts. These results indicate that θ_s and θ_k change significantly with frequency. However, if the frequency is fixed, θ_s and θ_k are largely independent of the electron energy varying from 1000 to 1 eV, as indicated by green arrows for parameters S and k in Figure 3B. This conclusion could also be obtained easily by analyzing the wavevectors of CR in Figure 2.

Figure 4A depicts the electron-velocity requirement for CR generation over the frequency range of 500–2000 cm^{-1}. As observed, CR generation occurs in the red- and blue-shaded hyperbolic-dispersion regions as well as the three gray-shaded elliptical-dispersion regions. Additionally, there exists a forbidden region of CR shaded in red oblique lines (ω = 828–851 cm^{-1}), wherein the iso-frequency contour is elliptical and CR generation condition ($v_0 > c/\sqrt{\varepsilon_x}$) cannot be met because ε_x lies in the range of 0–1. Four dotted lines indicating the electron velocities corresponding to electron energies E = 1000, 100, 10, and 1 eV go across the red- and blue-shaded regions, thereby predicting that, for low-energy electrons, there exist two radiation peaks over the entire frequency range.

Figure 4B depicts the simulated power spectra of CR generated using an electron bunch with energy of 1, 10, and 100 eV, and the same charge density (8×10^{-7} C/m^2) and electron–hBN gap (5 nm). The probes are located at positions $10 \times \lambda_{CR}$ (ω = 1500 cm^{-1}) below the hBN surface. The spectra demonstrate following properties. (1) There exist two peaks in accordance with the aforementioned prediction. (2) Lower electron energy produces higher-power CR, which has been reported in extant studies [16, 20]. In the results of this simulation, the CR power produced by the 1-eV electron bunch is roughly an order of magnitude higher than that produced by 100-eV electrons. (3) With reduction in electron energies, the spectrum peaks become blue- and red-shifted in the type-I and type-II regions, respectively [40].

3 Discussion

In this section, let us discuss the features of CR in hBN based on HPPs, compare CR generation from different mechanisms, and outlook the potential applications in the future.

Firstly, it can be seen that the basic rule for generating CR in a medium does not change, namely the electron velocity v_0 always exceeds the phase velocity of radiation, even though the electron energy decreases to 1 eV. This can easily be understood by comparing the wavevector k_e ($k_e = 2\pi \bullet f/v_0$ [18]) with k_{CR} in Figure 2. It can also be seen that the distinctive feature of CR is obvious from the equi-phase surfaces shown in Figure 3B,C, while there is a large angle between the directions of wavevector and Poynting vector shown in Figure 3B,C,E. Although in previous works low-energy electron excited radiation were studied theoretically and/or experimentally, such as the SPR based on nano-gratings [21], resonant transition radiation induced CR in photonic crystals [17], and the plasmonic radiation with an unchanged "Kelvin" angle on graphene [12], decreasing electron energy to such a low value has not been reported before to our best knowledge.

Secondly, let us compare the CR inside and on the surface of hBN film. When free electrons pass above the hBN film, volume CR and surface CR could be excited simultaneously. Besides the different regions they propagate in, other differences include: (1) In the propagation plane (x–z plane) of volume CR, the permittivity of hBN is anisotropic, and the IFC is hyperbolic as shown in Figure 2. However, in the propagation plane (y–z plane) of surface CR, the permittivity of hBN is isotropic, and the IFC of the surface CR is circular; (2) For surface CR, the directions of Poynting vectors and wavevectors are parallel (see Figures 3–5 in Ref. [40]). However, for volume CR, they are not parallel (see Figures 2 and 3).

Thirdly, the potential applications of CR-based HPP are anticipated. Although HPP is a promising candidate for applying in next-generation integrated photonic devices [30], existing HPP-launching approaches have low efficiency and high cost, because they rely on illuminating metal tips of an atomic force microscope [30] or other deep sub-diffraction nanostructures [49] using a mid-infrared laser. Moreover, launching HPPs with extremely large wavevectors is a major challenge for highly integrated HPP devices. For example, when employing the metal tip and sub-diffraction nanostructure, the largest wavevectors of HPP modes launched in hBN thin films are k_z/k_0 = 30 and k_z/k_0 = 28, respectively [30, 49]. Likewise, using the metal-tip launching approach in boron nitride nanotubes reveals the largest k_z/k_0 = 70 [35]. Results obtained in this study reveal that when employing a Cherenkov launching approach in hBN thin films, the wavevectors can be continuously tuned with the largest value of k_z/k_0 = 500 (because $k_z = k_e = 2\pi \bullet f/v_0$ [18] and $v_{1eV} = c/500$). In addition, the Cherenkov launching approach only using a low-energy free-electron source eliminates the needs for deep sub-diffraction nanostructures and mid-infrared lasers, which is highly cost-

effective. Besides the above application in integrated optical circuits, some applications can also be anticipated based on CR in mid-infrared. For examples, an integrated mid-infrared radiation source can be realized by extracting the radiation out from hBN, and as described by [36], the HPP-based CR in hBN can be used for on-chip near-field nano-imaging and infrared spectrometers.

Another interesting application concerns the attainment of a solid-state free-electron radiation source that is highly desired by scientists [50–54]. However, insufficient mobility of electrons and relatively strong thermal radiation are major obstacles in the realization of the said radiation sources [50, 55]. Based on the mechanism of CR generation in hBN films using extremely low-energy electrons, a hetero-structured hBN–graphene–hBN device might facilitate realization of the solid-state free-electron radiation source. Graphene provides quasi-free electrons with velocities of the order of the Fermi velocity $v_F = c/300$ (corresponding to free electrons with energy $E = 3$ eV) [56]. The two layers of hBN thin films serve as (1) an HPP-based CR-generation medium similar to that described in this paper, (2) encapsulating layers for improving the mobility of quasi-free graphene electrons [57], and (3) a pathway for transferring the heat generated in graphene to suppress thermal radiations [39]. By combining the advantages afforded by relatively high electron velocities in graphene [56] and extremely low electron velocity (energy) needed for CR generation in hBN, the desired result might be realized in the foreseeable future.

4 Conclusions

This study proposes a method for generating volume HPP-based CR in hBN using extremely low-energy free electrons. Owing to the small atomic-layer thickness and low optical damping, HPPs in hBN are superior to the plasmonic modes in HMMs. Analytical and numerical-simulation results obtained in this study reveal that the free-electron energy required for CR generation in hBN can be reduced to 1 eV in both type-I and type-II hyperbolic regions. Additionally, simulation results demonstrate that the CR power generated by electrons having 1-eV energy exceeds that generated by electrons having 100-eV energy. Another noteworthy indication is that HPPs over a considerably large range of wavevectors can be cost-effectively launched using the proposed free-electron excitation approach. By combining the approach with the high electron velocity of graphene, a new paradigm of solid-state free-electron radiation source might be realized in the near future. The authors believe that the findings of this study can potentially open new research avenues for CR and HPP applications.

Acknowledgment: The authors thank Zibo Qin, Dr. Yang Qing, Jinyu Li and Tianchang Li for their valuable discussions and helpful comments.

Author contributions: T.Q., F.L., and Y.L. conceived the study. T.Q. and Y.L. performed the theoretical and numerical analysis. T.Q., F.L., and Y.H. wrote the manuscript. Y.H. supervised the project. All authors reviewed and commented on the manuscript.

Research funding: National Key R&D Program of China (2018YFB2200402); National Natural Science Foundation of China (61575104, 61621064); Natural Science Foundation of Beijing Municipality (Z180012); Beijing Innovation Center for Future Chip; and Beijing Academy of Quantum Information Science.

Competing interests: The authors declare no competing financial interest.

References

[1] P. A. Cherenkov, "Visible emission of clean liquids by action of γ radiation," *Dokl. Akad. Nauk. SSSR*, vol. 2, p. 252, 1934.

[2] S. I. Vavilov, "On the possible causes of blue γ-glow of liquids," *Dokl. Akad. Nauk. SSSR*, vol. 2, p. 457, 1934.

[3] P. A. Cherenkov, "Radiation of particles moving at a velocity exceeding that of light, and some of the possibilities for their use in experimental," in *Nobel lectures, physics 1942-1962, 1998*, Singapore, World Scientific Publishing, pp. 426–441, 1998, https://doi.org/10.1142/3728.

[4] I. M. Frank, "Optics of light sources moving in refractive media," in *Nobel lectures, physics 1942-1962, 1998*, Singapore, World Scientific Publishing, pp. 442–469, 1998, https://doi.org/10.1142/3728.

[5] I. Y. Tamm, "General characteristics of radiations emitted by systems moving with super-light velocities with some applications to plasma physics," in *Nobel Lectures*, *Physics 1942-1962, 1998*, Singapore, World Scientific Publishing, pp. 470–483, 1998, https://doi.org/10.1142/3728.

[6] W. Galbraith, and J. V. Jelley, "Light pulses from the night sky associated with cosmic rays," *Nature*, vol. 171, pp. 349–350, 1953.

[7] F. Ciocci, A. Doria, G. P. Gallerano, et al., "Observation of coherent millimeter and submillimeter emission from a microtron-driven Cherenkov free-electron laser," *Phys. Rev. Lett.*, vol. 66, pp. 699–702, 1991.

[8] T. M. Shaffer, E. C. Pratt, and J. Grimm, "Utilizing the power of Cerenkov light with nanotechnology," *Nat. Nanotech.*, vol. 12, pp. 106–117, 2017.

[9] N. Kotagiri, G. P. Sudlow, W. J. Akers, and S. Achilefu, "Breaking the depth dependency of phototherapy with Cerenkov radiation and low-radiance-responsive nanophotosensitizers," *Nat. Nanotech.*, vol. 10, pp. 370–379, 2015.

[10] S. Liu, P. Zhang, W. Liu, et al., "Surface polariton Cherenkov light radiation source," *Phys. Rev. Lett.*, vol. 109, Art no. 153902, 2012.
[11] T. Zhao, R. Zhong, M. Hu, et al., "Cherenkov radiation via surface plasmon polaritons excitation by an electron beam in a layered metal-dielectric structure," *Eur. Phys. J. D.*, vol. 69, p. 120, 2015.
[12] X. Shi, X. Lin, F. Gao, H. Xu, Z. Yang, and B. Zhang, "Caustic graphene plasmons with Kelvin angle," *Phys. Rev. B*, vol. 92, Art no. 081404, 2015.
[13] I. Kaminer, Y. T. Katan, H. Buljan, et al., "Efficient plasmonic emission by the quantum Čerenkov effect from hot carriers in graphene," *Nat. Commun.*, vol. 7, Art no. ncomms11880, 2016.
[14] T. Zhao, M. Hu, R. Zhong, S. Gong, C. Zhang, and S. Liu, "Cherenkov terahertz radiation from graphene surface plasmon polaritons excited by an electron beam," *Appl. Phys. Lett.*, vol. 110, Art no. 231102, 2017.
[15] T. I. Andersen, B. L. Dwyer, J. D. Sanchez-Yamagishi, et al., "Electron-phonon instability in graphene revealed by global and local noise probes," *Science*, vol. 364, pp. 154–157, 2019.
[16] F. Liu, L. Xiao, Y. Ye, et al., "Integrated Cherenkov radiation emitter eliminating the electron velocity threshold," *Nat. Photon.*, vol. 11, pp. 289–292, 2017.
[17] X. Lin, S. Easo, Y. Shen, et al., "Controlling Cherenkov angles with resonance transition radiation," *Nat. Phys.*, vol. 14, pp. 816–821, 2018.
[18] F. J. García De Abajo, "Optical excitations in electron microscopy," *Rev. Mod. Phys.*, vol. 82, pp. 209–275, 2010.
[19] F. J. Garcıía de Abajo, "Multiple excitation of confined graphene plasmons by single free electrons," *ACS Nano,* vol. 7, pp. 11409–11419, 2013.
[20] Y. Yang, A. Massuda, C. Roques-Carmes, et al., "Maximal spontaneous photon emission and energy loss from free electrons," *Nat. Phys.*, vol. 14, pp. 894–899, 2018.
[21] A. Massuda, C. Roques-Carmes, Y. Yang, et al., "Smith–Purcell radiation from low-energy electrons," *ACS Photon.*, vol. 5, pp. 3513–3518, 2018.
[22] C. Roques-Carmes, S. E. Kooi, Y. Yang, et al., "Towards integrated tunable all-silicon free-electron light sources," *Nat. Commun.,* vol. 10, pp. 1–8, 2019.
[23] H. Ren, X. Deng, Y. Zheng, N. An, and X. Chen, "Nonlinear Cherenkov radiation in an anomalous dispersive medium," *Phys. Rev. Lett.*, vol. 108, Art no. 223901, 2012.
[24] S. V. Zhukovsky, O. Kidwai, and J. E. Sipe, "Physical nature of volume plasmon polaritons in hyperbolic metamaterials," *Opt. Express*, vol. 21, pp. 14982–14987, 2013.
[25] D. E. Fernandes, S. I. Maslovski, and M. G. Silveirinha, "Cherenkov emission in a nanowire material," *Phys. Rev. B*, vol. 85, Art no. 155107, 2012.
[26] A. Poddubny, I. Iorsh, P. Belov, and Y. Kivshar, "Hyperbolic metamaterials," *Nat. Photon.*, vol. 7, pp. 948–957, 2013.
[27] V. M. Shalaev, "Optical negative-index metamaterials," *Nat Photon*, vol. 1, pp. 41–48, 2007.
[28] K. Huang, "On the interaction between the radiation field and ionic crystals," *Proc. R. Soc. Lond. Ser. A Math. Phys. Sci.*, vol. 208, pp. 352–365, 1951.
[29] K. Huang, "Lattice vibrations and optical waves in ionic crystals," *Nature*, vol. 167, pp. 779–780, 1951.
[30] S. Dai, Z. Fei, Q. Ma, et al., "Tunable phonon polaritons in atomically thin van der Waals crystals of boron nitride," *Science*, vol. 343, pp. 1125–1129, 2014.
[31] A. J. Giles, S. Dai, I. Vurgaftman, et al., "Ultralow-loss polaritons in isotopically pure boron nitride," *Nat. Mater.*, vol. 17, pp. 134–139, 2018.
[32] J. D. Caldwell, A. V. Kretinin, Y. Chen, et al., "Sub-diffractional volume-confined polaritons in the natural hyperbolic material hexagonal boron nitride," *Nat. Commun.*, vol. 5, Art no. 5221, 2014.
[33] V. W. Brar, M. S. Jang, M. Sherrott, et al., "Hybrid surface-phonon-plasmon polariton modes in Graphene/Monolayer h-BN heterostructures," *Nano Lett.*, vol. 14, pp. 3876–3880, 2014.
[34] A. Woessner, M. B. Lundeberg, Y. Gao, et al., "Highly confined low-loss plasmons in graphene–boron nitride heterostructures," *Nat. Mater.*, vol. 14, pp. 421–425, 2015.
[35] X. G. Xu, B. G. Ghamsari, J.-H. Jiang, et al., "One-dimensional surface phonon polaritons in boron nitride nanotubes," *Nat. Commun.*, vol. 5, Art no. 4782, 2014.
[36] P. Li, M. Lewin, A. V. Kretinin, et al., "Hyperbolic phonon-polaritons in boron nitride for near-field optical imaging and focusing," *Nat. Commun.*, vol. 6, Art no. 7507, 2015.
[37] P. Li, I. Dolado, F. J. Alfaro-Mozaz, et al., "Infrared hyperbolic metasurface based on nanostructured van der Waals materials," *Science*, vol. 359, pp. 892–896, 2018.
[38] T. G. Folland, A. Fali, S. T. White, et al., "Reconfigurable infrared hyperbolic metasurfaces using phase change materials," *Nat. Commun.*, vol. 9, Art no. 4371, 2018.
[39] K.-J. Tielrooij, N. C. H. Hesp, A. Principi, et al., "Out-of-plane heat transfer in van der Waals stacks through electron–hyperbolic phonon coupling," *Nat. Nanotechnol.*, vol. 13, pp. 41–46, 2018.
[40] J. Tao, L. Wu, G. Zheng, and S. Yu, "Cherenkov polaritonic radiation in a natural hyperbolic material," *Carbon*, vol. 150, pp. 136–141, 2019.
[41] S. Adachi, *Optical properties of crystalline and amorphous semiconductors*. Boston, MA, Springer US, 1999, https://doi.org/10.1007/978-1-4615-5241-3.
[42] R. Geick, C. H. Perry, and G. Rupprecht, "Normal modes in hexagonal boron nitride," *Phys. Rev.*, vol. 146, pp. 543–547, 1966.
[43] Y. Cai, L. Zhang, Q. Zeng, L. Cheng, and Y. Xu, "Infrared reflectance spectrum of BN calculated from first principles," *Solid State Commun.*, vol. 141, pp. 262–266, 2007.
[44] J. Serrano, A. Bosak, R. Arenal, et al., "Vibrational properties of hexagonal boron nitride: inelastic X-ray scattering and Ab Initio calculations," *Phys. Rev. Lett.*, vol. 98, Art no. 095503, 2007.
[45] L. Britnell, R. V. Gorbachev, R. Jalil, et al., "Electron tunneling through ultrathin boron nitride crystalline barriers," *Nano Lett.*, vol. 12, pp. 1707–1710, 2012.
[46] CST, Particle Studio. Available at: https://www.cst.com.
[47] J.-K. So, F. J. García de Abajo, K. F. MacDonald, and N. I. Zheludev, "Amplification of the evanescent field of free electrons," *ACS Photon.*, vol. 2, pp. 1236–1240, 2015.
[48] H. Hu, X. Lin, J. Zhang, et al., Controlling Cherenkov threshold with nonlocality, 2020. Preprint arXiv:2002.04252.
[49] P. Pons-Valencia, F. J. Alfaro-Mozaz, M. M. Wiecha, et al., "Launching of hyperbolic phonon-polaritons in h-BN slabs by resonant metal plasmonic antennas," *Nat. Commun.*, vol. 10, Art no. 3242, 2019.
[50] S. A. Mikhailov, "Graphene-based voltage-tunable coherent terahertz emitter," *Phys. Rev. B*, vol. 87, Art no. 115405, 2013.
[51] M. Silveirinha, "A low-energy Cherenkov glow," *Nat. Photon.*, vol. 11, pp. 269–271, 2017.
[52] D. C. Tsui, E. Gornik, and R. A. Logan, "Far infrared emission from plasma oscillations of Si inversion layers," *Solid State Commun.*, vol. 35, pp. 875–877, 1980.

[53] A. Friedman, A. Gover, G. Kurizki, S. Ruschin, and A. Yariv, "Spontaneous and stimulated emission from quasifree electrons," *Rev. Mod. Phys.*, vol. 60, pp. 471–535, 1988.
[54] R. A. Höpfel, E. Vass, and E. Gornik, "Thermal excitation of two-dimensional plasma oscillations," *Phys. Rev. Lett.*, vol. 49, pp. 1667–1671, 1982.
[55] S. A. Mikhailov, "Plasma instability and amplification of electromagnetic waves in low-dimensional electron systems," *Phys. Rev. B*, vol. 58, pp. 1517–1532, 1998.
[56] K. S. Novoselov, A. K. Geim, S. V. Morozov, et al., "Two-dimensional gas of massless Dirac fermions in graphene," *Nature*, vol. 438, pp. 197–200, 2005.
[57] M. A. Yamoah, W. Yang, E. Pop, and D. Goldhaber-Gordon, "High-velocity saturation in graphene encapsulated by hexagonal boron nitride," *ACS Nano*, vol. 11, pp. 9914–9919, 2017.

Supplementary Material: The online version of this article offers supplementary material (https://doi.org/10.1515/nanoph-2020-0090).